# Photodissociation of Trapped Metastable Multiply Charged Anions: A Routine Electronic Spectroscopy of Isolated Large Molecules?

**Mattias Kordel,[†] Detlef Schooss,[†] Stefan Gilb,[‡,§] Martine N. Blom,[†] Oliver Hampe,*[,†] and Manfred M. Kappes[†,‡]**

*Institut für Nanotechnologie, Forschungszentrum Karlsruhe, P.O. Box 3640, D-76021 Karlsruhe, Germany, and Institut für Physikalische Chemie, Universität Karlsruhe, Kaiserstraβe 12, D-76128 Karlsruhe, Germany*

*Received: February 18, 2004; In Final Form: April 2, 2004*

Electron loss and dissociation occur upon optical excitation of tetraanionic phthalocyanines trapped in a Fourier transform ion cyclotron resonance (FT-ICR) mass spectrometer. Experiments were carried out by irradiating at 355 nm and between 570 and 695 nm covering the Q band region of phthalocyanines. Laser fluence dependencies show a two-photon-process as the underlying absorption law for the observed decay which corresponds to an unexpectedly low kinetic shift given the 69-atom-size of this molecule and the activation energies expected for the decay channels. We assign this effect to the pronounced electronic metastability of these 4-fold negatively charged ions. Electronic excitation is associated not only with thermal ionization but also with a corresponding increase in the tunneling autodetachment rate.

## 1. Introduction

Photodissociation spectroscopic probes of molecular ions trapped in ICR cells[1] date back to the early 1970s and are closely connected to pioneering work in the groups of Dunbar[2] and Beauchamp.[3] Since then, the advancement of ion sources and trap technologies, and the advent of novel tuneable laser light sources have made electronic photodissociation probes of small organic and organometallic radical ions stored in Penning traps almost routine.[4,5,6] However, electronic photodissociation spectroscopy in Penning traps has only rarely been applied to characterize ions with more than 20 atoms, because the method, as applied to large ions, suffers from the dual problems of kinetic shift and blackbody radiative cooling.

Blackbody radiative cooling ensures that excited ion ensembles relax to trap temperature on time scales faster than seconds. If no dissociative decay has occurred on this time scale, light absorption will go undetected.[7,8] In order for decay to be measurable (e.g. via a change in mass-to-charge ratio) within this "blackbody" time window, overall excitation energies significantly above the dissociation threshold are required to compensate for the pertaining kinetic shift. Given the same activation energies, the amount of excitation energy required to overcome the kinetic shift increases rapidly with molecular size. High excitation energies can in turn only be provided by higher order sequential multiphoton absorption processes. As a consequence, the ion ensemble generated by the laser pulse may initially contain a wide and generally unknown distribution of differently excited species, as governed by the photon flux and the unknown sequential photon absorption cross sections. One then expects to find a broadening of absorption bands due to increasing vibrational excitation as the number of previously absorbed photons is raised and the excitation energy is redistributed in the molecule.

The latter qualitative arguments are of course dependent in detail on the relevant decay processes, their threshold energies and the underlying vibrational density of states. For example, blackbody radiative decay may compete with electron loss. A quantitative example serves to illustrate this point: $C_{60}^-$ has an electron detachment energy of 2.67 eV. Recent measurements of $C_{60}^-$ thermalized to room temperature in an ion storage ring have shown that for an electron emission rate significantly faster than initial blackbody radiative relaxation to be reached about 14 eV of additional energy are necessary, which have to be provided by sequential photon absorption.[9] In such a situation, the sequential absorption cross sections can only be determined by using certain model assumptions. Correspondingly, it is difficult to accurately obtain a wavelength-dependent visible-near-IR absorption cross section for the first of several photons.

In this contribution, we explore this problem in the context of multiply negatively charged species. Multiply charged anions (MCAs) are of particular present interest as their Coulomb barrier gives rise to a number of new phenomena. Several recent photodetachment spectroscopic studies have for example proven the existence of MCAs having *negative* electron detachment energies. These include small five-atomic dianions $PtCl_4^{2-}$,[10] large metalorganic ions such as metal phthalocyanine tetraanions,[11] or DNA oligonucleotides.[12] Due to this negative electron binding energy, some of these metastable MCAs have been shown to decay spontaneously at room temperature by means of electron tunneling autodetachment[13] on a second timescale. It appears that tunneling autodetachment is a general phenomenon for metastable MCAs; however, the rates are expected to vary widely. As yet, the influence of vibrational excitation on the autodetachment rate of MCAs remains to be understood in detail. Furthermore, it is not clear presently to what degree electronic excitation influences (subsequent) tunneling emission and therefore whether the effect could be used for spectroscopic characterization of large multianions in the context of depletion measurements. Here, we present a detailed

* To whom correspondence should be addressed. E-mail: Oliver.Hampe@int.fzk.de. Fax: +49 (0)7247-826368.
† Forschungszentrum Karlsruhe.
‡ Universität Karlsruhe.
§ Current address: Department of Chemistry, University of California, Berkeley, CA 94720-1460.

10.1021/jp049261b CCC: $27.50 
Published on Web 05/07/2004

FT-ICR laser spectroscopic study with the aim of obtaining answers to these questions. Phthalocyanine tetrasulfonate tetraanions are excellent probe systems owing to their known negative fourth electron affinities[11,14] and strong visible-near UV absorptions.

## 2. Experimental Section

**2.1. Ion Generation and Trapping.** The experiments were carried out in a Fourier transform ion cyclotron resonance mass spectrometer (BioApex II, Bruker Daltonics, Billerica, MA), which has been described in detail recently.[15] Briefly, it is equipped with a 7 T superconducting magnet and a cylindrical ICR cell (Infinity cell). The ions were formed in an electrospray source (Analytica of Branford) from aqueous solutions of the following sulfonated phthalocyanines: $MPc(SO_3Na)_4$, M = Ni, Cu; and $H_2Pc(SO_3H)_4$ with Pc = phthalocyanine. The copper phthalocyanine was purchased from Sigma-Aldrich, the nickel phthalocyanine was a kind gift from Prof. Johan van Lier (University of Sherbrooke, Canada), and the free base phthalocyanine was purchased from Frontier Scientific Europe Ltd. (Carnforth, U.K.). All phthalocyanine samples are constituted from a mixture of regioisomers with respect to the position of the four sulfonate groups on the benzoannulated pyrrole rings.[14] Solutions of typically 0.5−1 mmol/L were sprayed at 0.2 mL/h through stainless steel capillaries held at ground potential employing nitrogen as spraying gas. The desolvation process through a 0.6 mm i.d. glass capillary was enhanced by a counterflow of nitrogen drying gas heated to about 200°C.

Negative ions thereby brought into the gas-phase were pretrapped in a hexapole ion trap (run at a fixed frequency of 5.3 MHz with variable amplitude of up to 600 $V_{p-p}$) for typically 0.5 s before being pulsed into the ICR cell via a high voltage ion transfer. A rough pre-isolation of the desired species $MPc(SO_3)_4^{4-}$ was achieved by choosing an appropriate hexapole rf voltage, due to the fact that the $MPc(SO_3)_4^{4-}$ ions had the lowest *m*/*z* ratio of all species present in the hexapole trap. By lowering the rf voltage $V_{p-p}$ to about 40 V, almost all ions with higher *m*/*z* ratios were ejected from the hexapole ion guide; that is, the ion guides high mass cutoff was used.[16] For ICR trapping, the entrance electrode was pulsed open to ground potential for 0.8−0.9 ms in order to allow ions to enter the trap. Since this transfer time is somewhat sensitive to the *m*/*z* value of the ions, it provides a rudimentary time-of-flight mass spectrometer, and we exploited this effect to further discriminate the $MPc(SO_3)_4^{4-}$ species from unwanted ions.

The isolation of the tetraanion was completed in the ICR cell by resonantly ejecting the remaining unwanted ions from the trap by means of radial dipolar rf excitation. This procedure was applied in the first set of experiments where we investigated the size of the ion cloud as well as various fragmentation channels and laser power dependency. However, for acquiring spectral data using an optical parametric oscillator (OPO) laser, this last isolation step turned out to be disadvantageous in terms of reduced spatial overlap between the laser beam and the ion cloud and was therefore omitted.

**2.2. Laser System and Optical Setup.** For the measurements at 355 nm, we used the third harmonic of a Nd:YAG pulse laser (Continuum Electrooptics, Powerlite 8030) with a repetition rate of 30 Hz and a pulse length of approximately 7 ns. The laser beam was synchronized to the experimental sequence of the mass spectrometer by an electronic shutter (Newport 845/846 HP) and deflected twice by 90° first with a dielectric mirror and then with a prism before being coupled into the Penning trap in opposite direction to the ion beam through a quartz window. Owing to the good profile and low divergence of the Nd:YAG laser beam it was used without any further shaping or focusing.

For the spectral data, an OPO laser (Continuum Electrooptics, Panther) was used that was pumped by the aforementioned Nd:YAG laser at an average energy of 125 mJ/pulse yielding OPO laser pulse energies of 25 mJ at $\lambda = 450$ nm and 10 mJ at $\lambda = 600$ nm. To take power dependencies at various wavelengths, the laser beam was attenuated by means of a polarization attenuator. For online measurements of the relative laser power, we guided a reflection from a beam splitter onto a pyroelectric detector (Coherent 33−1140) read out by an oscilloscope (LeCroy, Waverunner LT322) when using the Nd:YAG laser or by a power monitor (Coherent, Fieldmaster GS) when using the OPO system. The vertically very divergent output of the OPO was corrected for by a cylindrical lens ($f = 750$ mm) and focused through the shutter by a spherical lens ($f = 100$ mm). Behind the shutter, the beam was further shaped by a 3-fold telescope which was optimized with respect to optimum overlap with the ion cloud. Best overlap was achieved by maximizing the depletion of the parent ion signal. To attenuate the OPO laser beam, a Berek compensator (New Focus, Model 5540) as a variable waveplate and a glan laser prism (Linos Photonics) acting as a polarization analyzer were brought into the beam path. Rotation of the compensator was automated by using a motor-driven rotational stage (New Focus, model 8401M).

To determine the profile of the ion cloud in the ICR cell, a slit aperture of 0.3 mm width and 5 mm height was mounted vertically behind the deflecting prism on a horizontally adjustable linear stage, so that the laser beam could be scanned across the trap entrance and exit holes of 6 mm diameter ensuring constant incident angle and laser fluence. We scanned the laser across the trap opening by moving prism and slit aperture horizontally in steps of 0.25 mm for a coarse run and with step sizes of 0.125 mm in the region of the center of the trap. The laser beam profile was measured by deflecting the full beam onto a beam profiler (Ophir Optronics, Beamstar). The beam profiler was positioned at a distance corresponding to the laser beam path into the center of the Penning trap to map the actual profile at the location of the ion cloud.

For wavelength dependent scans, the OPO laser was operated under its own software control. The absolute wavelength of the laser was independently determined with a calibrated wavemeter (Atos, LRL-005) in several measurements on different days. Wavelength scans obtained prove that the reproducibility of the laser stepper motor control is better than 0.1 nm.

**2.3. Computer Control and Data Aquisition.** The FT ICR mass spectrometer runs under the control of Bruker's software package xmass (version 6.0) that was interfaced by us in order to control the external devices (laser, power meter, and laser attenuator) by means of serial ports (RS232). The experimental cycles were controlled by Tcl scripts developed in our group and implemented into the xmass software allowing us to fully automate the experiments.[17] For all wavelength and power dependent data, typically 64 or 128 mass spectra were accumulated at each point to obtain sufficiently good statistics. Each of these steps was followed by a reference measurement without laser irradiation under otherwise identical conditions in order to account for fluctuations in the ion source stability. Intensities of ion signals were taken as integrals of the corresponding peaks in the mass spectra in the frequency domain and corrected for their respective charge state. In the following, $I/I_0$ denotes the ratio of ion intensities obtained with and without laser beam. This ratio is referred to as depletion or action ratio

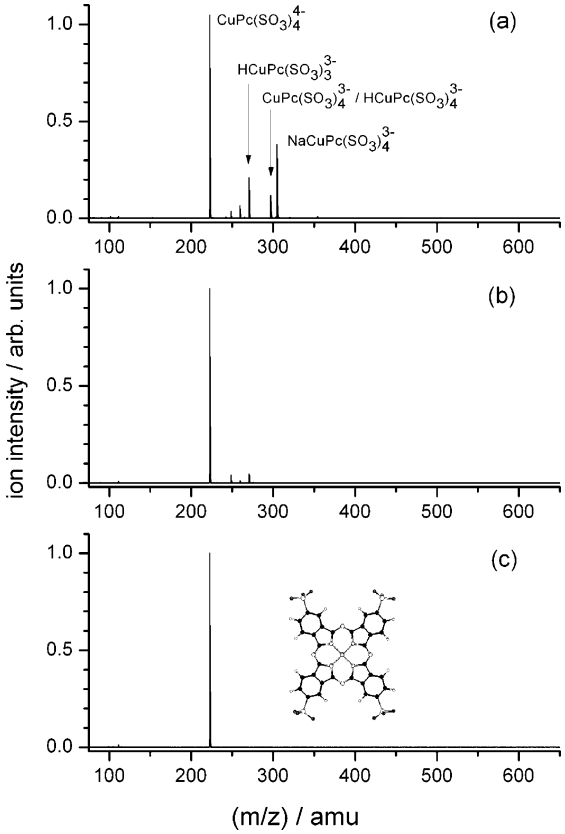


**Figure 1.** Negative ion FT-ICR mass spectra from a sprayed solution of $CuPc(SO_3)_4Na_4$ optimized to give optimum tetraanion signal (a), preselected to discriminate against higher *m*/*z* ions (b) and isolated in the ICR cell (c). Also shown is a molecular structure of tetraanionic $CuPc(SO_3)_4^{4-}$ [$CuC_{32}H_{12}N_8(SO_3)_4^{4-}$] as the $D_{2h}$ isomer with respect to the position of the sulfonate groups.

if *I* marks the intensity of the parent or a fragment ion, respectively.

## 3. Results and Discussion

**3.1. ESI Mass Spectra and 355 nm Photodissociation.** Figure 1 shows typical mass spectra upon spraying solutions of $CuPc(SO_3)_4Na_4$ as trapped (a) and with preselection (b). The enrichment of the desired tetraanionic species at $m/z = 223$ in the ICR cell is evident and can be completed by ejecting the remaining trianions by means of resonant shots at the appropriate cyclotron frequencies (Figure 1c). Also included in Figure 1c is the molecular structure of a metal phthalocyanine tetrasulfonate tetraanion (shown is the $D_{2h}$ isomer with respect to the position of the $SO_3^-$ groups).

Figure 2 shows a typical mass spectrum taken after irradiating the isolated precursor $CuPc(SO_3)_4^{4-}$ in the ICR trap with a single laser pulse at 355 nm at a pulse energy of 7 mJ corresponding to a photon flux of 3.5 $Å^{-2}$. Very heavy fragmentation is apparent after the measurement time delay of 10 ms. Products formed include various singly, doubly, and triply charged species. The most prominent fragments observed upon 355 nm irradiation are summarized in Table 1. Interestingly, all fragments observed had a fully intact metal phthalocyanine core; that is, fragmentation takes place exclusively at the sulfonate groups of the molecule. Measurements at low laser fluence suggest that the lowest energy relaxation process upon photon absorption is electron detachment which leads to a $CuPc(SO_3)_4^{3-}$ ionic species (eq 1). Note, that electron loss decay at room temperature, though much slower, has also been observed in

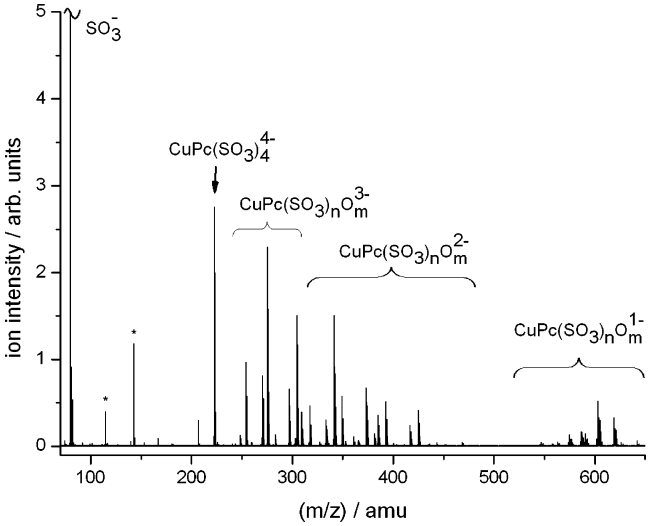


**Figure 2.** Photodissociation mass spectrum of the parent ion $CuPc(SO_3)_4^{4-}$ taken at 355 nm (pulse energy of 7 mJ). Note, that all fragment ions observed comprise an intact metal phthalocyanine core. The most prominent fragment ions are assigned in Table 1.

**TABLE 1: Ionic Fragments Observed upon Photoexcitation at 355 nm of the Isolated Parent Ion $CuPc(SO_3)_4^{4-}$**

| charge state | fragment | *m*/*z* in amu |
|---|---|---|
| 3 | $CuPc(SO_3)_4^{3-}$ | 297.0 |
| | $CuPc(SO_3)_3O^{3-}$ | 275.6 |
| | $CuPc(SO_3)_3^{3-}$ | 270.3 |
| | $CuPc(SO_3)_2O_2^{3-}$ | 254.3 |
| 2 | $CuPc(SO_3)_2O^{2-}$ | 373.5 |
| | $CuPc(SO_3)_2O_2^{2-}$ | 381.5 |
| | $CuPc(SO_3)O_3^{2-}$ | 349.5 |
| | $CuPc(SO_3)O_2^{2-}$ | 341.5 |
| | $CuPc(SO_3)O^{2-}$ | 333.5 |
| | $CuPcO_4^{2-}$ | 317.5 |
| | $CuPcO_3^{2-}$ | 309.5 |
| 1 | $CuPcO_3^-$ | 619.0 |
| | $CuPcO_2^-$ | 603.0 |
| | $SO_3^-$ | 80.0 |

the absence of light as has been reported previously[14] and is due to the metastability of the tetra-anionic species. Closer inspection of the photofragmentation mass spectra reveals that the prominent dissociation channels after electron loss are fragmentation loss of $SO_3^-$ (eq 2) and of a neutral $SO_2$ unit (eq 3)

$$CuPc(SO_3)_4^{4-} \rightarrow CuPc(SO_3)_4^{3-} + e^- \quad (1)$$

$$CuPc(SO_3)_4^{4-} \rightarrow CuPc(SO_3)_3^{3-} + SO_3^- \quad (2)$$

$$CuPc(SO_3)_4^{3-} \rightarrow CuPc(SO_3)_3O^{3-} + SO_2 \quad (3)$$

Since fragmentation may occur within the time scale of the laser pulse, it cannot be ruled out that the fragments may absorb further photons, obstructing a complete picture of the fragmentation pathways. We discuss the fluence dependent fragment yields in more detail in section 3.3.

**3.2. Ion Cloud Profile.** We did several measurements to evaluate the ion distribution in the ICR cell as described in the Experimental Section. Figure 3 displays the data points as a typical outcome of such a scan indicating a bimodal radial distribution. We attribute the differing heights of the maxima to a slightly imperfect laser beam alignment with respect to the cell axis. However, the dip in the center of the curve was

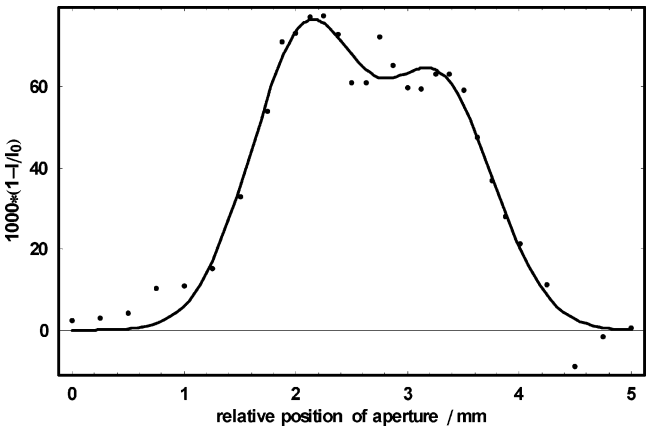


**Figure 3.** Ion cloud distribution in the Penning trap as measured by the fragment ion intensities as a function of relative laser position across the ICR cell (experimental points shown as dots). The distribution appears to be bimodal (solid line is a best fit using two Gaussians).

perfectly reproducible in several measurements indicating a projected ion density distribution with a local minimum on the trap axis.

Due to the superposition of the ion's cyclotron and magnetron motion in an ICR cell, one expects in fact a donut shaped ion distribution, when it is projected onto a plane perpendicular to the magnetic field axis. Therefore, we took a superposition of two Gaussian functions to describe the profile of this projected donut distribution. We allowed the parameters $A$ and $B$ (maxima of the Gaussians) to differ in order to give a better fit while using the same width $\sigma$ for both Gaussians. The function then reads

$$f(x) = A\exp\left\{-\frac{(x-x_{01})^2}{2\sigma^2}\right\} + B\exp\left\{-\frac{(x-x_{02})^2}{2\sigma^2}\right\} \quad (4)$$

where $x_{01}$ and $x_{02}$ are the positions of the maxima. This function was convoluted with a boxcar function to account for the finite slit aperture with unit height, leading to

$$h(x) = \sqrt{\frac{\pi}{2}}\sigma\left[A\left(\mathrm{erf}\left\{\frac{w+(x-x_{01})}{\sigma\sqrt{2}}\right\} + \mathrm{erf}\left\{\frac{w-(x-x_{01})}{\sigma\sqrt{2}}\right\}\right) + B\left(\mathrm{erf}\left\{\frac{w+(x-x_{02})}{\sigma\sqrt{2}}\right\} + \mathrm{erf}\left\{\frac{w-(x-x_{02})}{\sigma\sqrt{2}}\right\}\right)\right] \quad (5)$$

where erf is the error function and $w$ is the half width of the aperture. The solid line in Figure 3 is a least-squares fit of eq 5 to the data points.

The most interesting parameters resulting from the fit are the distance between the two maxima, which is tentatively interpreted as the diameter of the magnetron motion, and the half width of the Gaussians interpreted as the cyclotron radius. We obtain 0.6 mm for the magnetron radius and 0.48 mm for the cyclotron radius. These values are in good agreement with trajectory simulations[18] employing SIMION[19] for ions with a kinetic energy of approximately 10 eV. In total, the diameter of the ion cloud in the ICR cell under our experimental conditions was determined to be 2.2 ± 0.1 mm which is a promising result in order to do gas phase spectroscopy where high ion densities are called for to be able to measure even small absorption cross sections with currently available laser pulse energies.

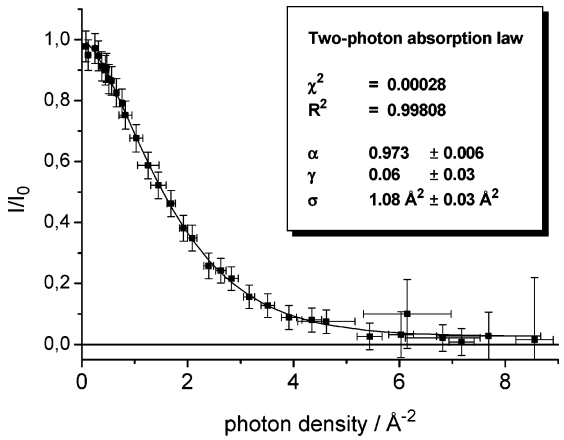


**Figure 4.** Laser fluence dependence of the parent ion depletion at 355 nm. Superimposed is a two photon absorption law with equal cross sections fitted to the data points (eq 6 in the text) with fit parameters obtained.

**3.3. Laser Power Dependencies and Kinetic Modeling.** Power dependence measurements were carried out at 355 nm (the third harmonic wavelength of the Nd:YAG laser), which is close to the B (or Soret) band of phthalocyanines in solution. This type of experiment is important in order to give intrinsic information on the power law operative for the dissociation process as well as to determine the experimental overlap parameter between laser and ion cloud. Figure 4 shows a typical power dependence given as the depletion ratio of the parent ion $CuPc(SO_3)_4^{4-}$ as a function of laser fluence. An inverse Beer−Lambert absorption law[20] was fitted to the data which includes an overlap parameter $\alpha$ and a branching ratio $\gamma$ denoting the fraction of ions which fragment after having absorbed one photon. Correspondingly, the fraction $(1-\gamma)$ requires two photons to dissociate. The dissociation cross section $\sigma$ was assumed to be equal for the first and the second photon. The absorption law then reads[20]

$$\frac{I}{I_0} = 1 - \alpha + \alpha(1 + (1-\gamma)\sigma F)\exp(-\sigma F) \quad (6)$$

where $F$ is the photon density (i.e., the number of photons per unit area and laser pulse). The quality of the fit shows a very good agreement between our data and the absorption law given by eq 6. The resulting value for $\alpha$ of 0.973 ± 0.006 proves the excellent overlap; that is, essentially all ions in the trap can be photodissociated by a single laser shot. The small value for $\gamma$ is indicative of an overall 2-photon-absorption process responsible for the dissociation. From this fit, the absorption cross section is evaluated to be $\sigma = 1.08 \pm 0.03$ Å$^2$.[21] Within an absolute error of 50% that we assign to our value, it agrees with extinction data from UV−vis absorption spectra that we have taken in solution.

It is instructive to examine the power dependencies of the individual fragments in some more detail. Figure 5, parts a and b, displays the action power dependences for the triply and doubly charged fragments, respectively. Apparently, the occurrence of triply charged species peaks around photon densities of 2 Å$^{-2}$, whereas the intensities of the doubly charged ions have a maximum around 3−3.5 Å$^{-2}$. To rationalize these, we now outline a very simple kinetic model to describe the overall fragmentation power dependence. It is based on multiple photon absorption as a statistical process preceding the dissociation of the hot molecular ion. This picture of the absorption process implies that the intramolecular repartitioning of the energy is

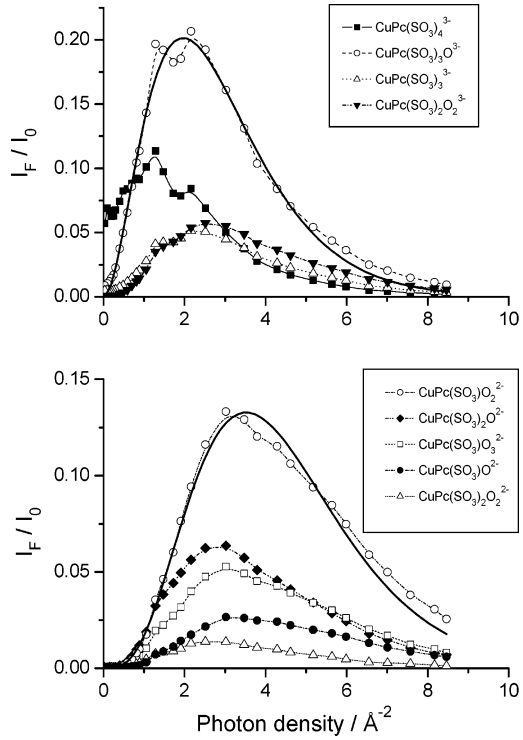


**Figure 5.** Laser fluence dependence of the major fragment ions including triply charged anions (top panel) and doubly charged ions (bottom panel). Thick solid lines represent Poisson distributions (eq 7 in the text) fitted to each one dataset indicating a 2- and 4-photon process for trianions and dianions, respectively (see text for details). Note that the finite signal of trianionic $CuPc(SO_3)_4^{3-}$ for zero fluence is attributable to the (spontaneous) electron autodetachment from the metastable parent tetraanion, as reported previously.[14]

faster than the time between absorption steps and that the absorption cross section is little dependent on the temperature of the ion.[22] Taking therefore the absorption cross sections $\sigma$ for all sequential steps to be constant, one obtains a Poisson distribution for the number $k$ of absorbed photons. The relative number of molecules $N(k)$ as function of laser fluence $F$ then reads

$$\frac{N(k)}{N(0)} = c\frac{1}{k!}(\sigma F)^k \exp(-\sigma F) \qquad (7)$$

If we enter the value obtained above from the depletion data of $\sigma = 1.07$ Å$^2$ into eq 5 and include a scaling factor $c$, we end up with a fit function with $k$ as the only free parameter.

The result of such a fit is included in parts a and b of Figure 5 (bold and solid lines) for the examples of one triply and one doubly charged fragment, respectively. Consistent with the depletion data, we obtain values close to $k = 2$ for the trianion and $k = 4$ for the dianion. This suggests a remarkable result: on average, two photons of 3.49 eV suffice to induce a primary electron loss and subsequent fragmentation of this large molecule.

**3.4. Direct Photodetachment vs Statistical Electron Emission.** Of particular interest is the initial decay step of electron loss. As has been shown previously in photoelectron spectroscopic studies of this molecule,[14,23] it is possible to directly photodetach an electron with 355 nm radiation, and the associated Coulomb barrier was suggested to be about 2.8 eV. Given the much larger effective cross sections determined here compared to those expected for direct photodetachment, our experiment is obviously sensitive to an additional slow electron loss channel (reflecting the much longer experimental time scales available compared to the PES studies). Thus, we assume that the electronically excited state relaxes into the vibrational manifold of states of the ground electronic state on a time scale faster than the laser pulse length of 7 ns, i.e., before the second photon is absorbed. One might wonder whether a completely statistical electron emission from a hot molecule can be invoked to describe the observed effect. Klots' theory expresses the rate constant $k(T)$ for such a process as a function of the absolute temperature $T$[24,25]

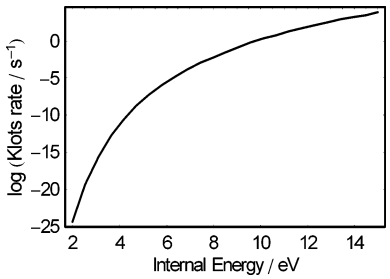


**Figure 6.** Calculated statistical electron emission rate (following Klots' theory, see text eq 8) as a function of internal energy for a laser-heated CuPc tetraanion assuming a barrier height of 2.8 eV.

$$k(T) = (2k_BT/h)(2m_eR_{max}{}^2k_BT/\hbar^2)(g_f/g_i)\exp(-E_b/k_BT) \qquad (8)$$

where $k_B$ denotes the Boltzmann constant, $E_b$ is the energy (Coulomb) barrier for electron emission, and $m_e$ is the electron mass. Since copper phthalocyanine tetrasulfonate has an open shell electronic ground state (spin dublet), the ratio of the electronic degeneracies $g_f/g_i$ of final and initial states (here trianion and tetraanion, respectively) is expected to be 0.5. $R_{max}$ corresponds to an classical hard sphere radius of the molecule for electron emission/attachment that we estimate to be 500 pm as described recently.[14] To map this temperature-dependent rate onto an energy scale, we use the microcanonical definition of temperature

$$\frac{1}{k_BT} = \frac{\mathrm{d}\ln\Omega}{\mathrm{d}E} \qquad (9)$$

with $\Omega = \rho(E)\,\mathrm{d}E$.

The vibrational density of states $\rho(E)$ was obtained from the frequency spectrum of $CuPc(SO_3)_4^{4-}$ as calculated at PM3 level using the HyperChem program package.[26] The frequencies of all vibrational modes were taken to calculate a density of states by means of the Haarhoff approximation.[27,28] The resulting Klots rate is shown in Figure 6 as a function of internal energy stored in the molecule. The internal energy of the photoexcited molecular ion is given as the sum of the ions energy at room temperature which amounts to 1.3 eV and the energy of the photons absorbed. We conclude that under these conditions absorption of two 355 nm photons (=7 eV) would not sufficiently heat the molecule to cause an over-the-barrier electron loss on the time scale of our experiment, if we assume a barrier height of 2.8 eV. Rather, it would take about 12 eV of internal energy to be able to detect thermal electron emission on the time scale of our FT-ICR experiment.

Alternatively, one might propose from our results a significantly smaller barrier than previously assumed: a Coulomb barrier of $2.1 \pm 0.1$ eV and an internal energy of 8.3 eV would lead to a Klots rate within our experimental time window of about 10 ms. However, this proposition seems unlikely since even at much smaller photon energies of 1.88 eV (660 nm) two photon excitation still leads to measurable electron emission

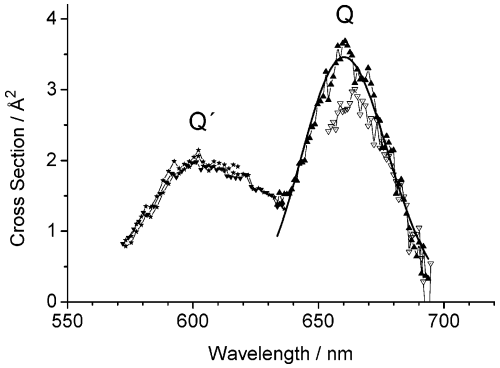


**Figure 7.** Photodepletion cross section of $CuPc(SO_3)_4^{4-}$ as a function of excitation wavelength assuming a two-photon absorption process. Different symbols correspond to independent measurements. A Gaussian fit to the Q band is shown as solid line.

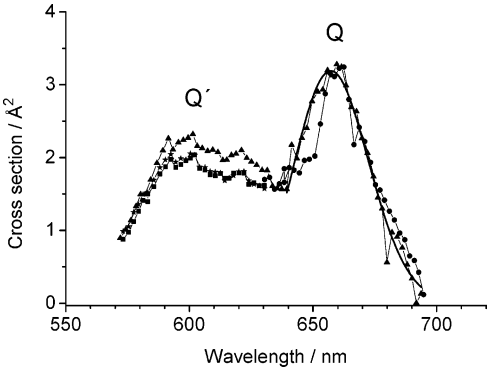


**Figure 8.** Photodepletion cross section of $NiPc(SO_3)_4^{4-}$ as a function of excitation wavelength assuming a two-photon absorption process. Different symbols correspond to independent measurements. A Gaussian fit to the Q band is shown as solid line.

and fragmentation (see paragraph 3.5). Other mechanisms possibly contributing to autodetachment beyond "classical" thermoionization include (i) vibrationally enhanced ground state tunneling emission (after internal conversion) and (ii) tunneling emission from an electronically excited state, as has been suggested recently.[23]

**3.5. Spectral Photofragmentation Data.** Based on the promising results of the 355 nm photoexcitation experiments, the photodepletion studies were extended to the wavelength range where the Q bands of these molecules are to be expected (based on solution spectra) to test the possibility of readily obtaining electronic absorption spectra in gas-phase.

Further fluence dependence depletion measurements at 608, 638, and 660 nm (not shown) were recorded to check for the correct absorption law. The results of the analysis are again in very good agreement with a two-photon absorption law as given by eq 6 assuming equal cross sections for the first and second photon. We also tested a two-photon-absorption law with differing cross sections ($\sigma_2 \neq \sigma_1$).[29] The fit results do not lead to a significantly better $\chi^2$ confidence for this model. We checked carefully, however, that peak position and the peak width are essentially identical (within experimental errors) for the two deconvolution procedures whereas the absolute cross sections turned out to vary by almost a factor of 2, being the main contribution to the absolute error that we assign. We therefore proceed to discuss the data analyzed on the grounds of the 2-photon-model with equal cross sections.

Due to the strongly nonhomogeneous beam profile of the OPO laser, we also monitored the beam profile in steps of 10 nm. The profile can be approximated by a two-dimensional ellipsoid. These profiles were taken into account to deconvolute the data to obtain photodissociation cross sections as outlined in the appendix. Together with an overlap parameter $\alpha = 1$, which was checked experimentally to ensure near complete depletion at high laser power, the two-photon model then reads

$$\frac{I}{I_0} = \int_{-\infty}^{\infty}\int_{-\infty}^{\infty} \rho(x,y)\left(1 + \sigma\frac{P}{h\nu}\Phi(x,y)\right) \times \exp\left\{-\sigma\frac{P}{h\nu}\Phi(x,y)\right\} \mathrm{d}x\,\mathrm{d}y \quad (10)$$

where $P$ is the integral laser pulse energy, $\nu$ is the frequency of the laser light, and $h$ is the Planck constant.

Figures 7−9 reproduce photodepletion spectral scans of $CuPc(SO_3)_4^{4-}$, $NiPc(SO_3)_4^{4-}$, and $H_2Pc(SO_3)_4^{4-}$, respectively, in the range from 540 nm (2.3 eV) to 695 nm (1.78 eV). For each of the molecules, these scans were taken at least twice on different days, indicated by the different datasets in the graphs

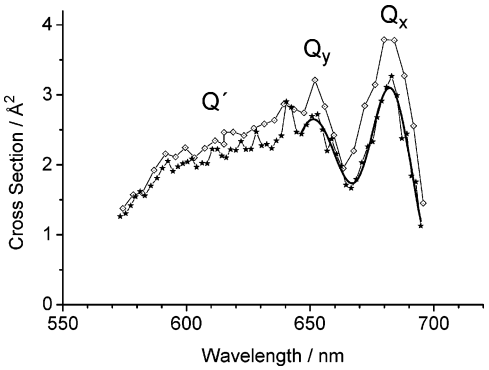


**Figure 9.** Photodepletion cross section of $H_2Pc(SO_3)_4^{4-}$ as a function of excitation wavelength assuming a two-photon absorption process. Different symbols correspond to independent measurements. A Gaussian fit to the Q band is shown as solid line.

which are shown without any scaling. For the two metal phthalocyanines, one recognizes two fairly broad features (labeled Q and Q′), whereas for the free base phthalocyanine, we assign three features. For a consistent parametrization of the spectroscopic bands, a Gaussian (two Gaussians in the case of $H_2Pc$) envelope is fitted to the lowest energy feature and included in Figures 7−9. Peak position and width from this fitting procedure are summarized in Table 2. An assignment of the lowest energy band (or Q band) found for the tetraanionic phthalocyanines is given based on the work by Edwards and Gouterman on the neutral analogues.[30] Compared to their absorption data in the vapor phase taken at about 500 °C, the position of the Q band is slightly red-shifted (by less than 6 nm) for both of the two metal phthalocyanine ions. As in the neutral vapor phase measurements, nickel and copper phthalocyanine ions almost coincide in their Q band positions, whereas the lowest energy transition for the free base phthalocyanine ion is red-shifted by about 30 nm (see Table 2).

In general, our spectra are considerably narrower in bandwidth compared to the neutral molecule data, as would be expected for the (lower) room-temperature measurement. The Q band is split for the free base phthalocyanine into a $Q_x$ and $Q_y$ band which arise from the reduced symmetry compared to metal phthalocyanines. This is also reproduced in our photodepletion measurement for the anion and compares well with laser induced fluorescence data taken in inert gas[31] and Shpol'skii matrices.[32] There, it was possible to obtain resolved vibronic transitions allowing assignments of band origins at 677 and 694 nm for $Q_x$ and at 634 and 655 nm for $Q_y$, again in good agreement

**TABLE 2: Spectral Data of the Low Energy Electronic Absorption Band (Q Band) of Tetrasulfonated Phthalocyanine Tetraanions Derived from Mass-Selected Photodepletion Measurements (See Figures 7−9)**

| | | Q band position in nm (eV) | bandwidth in nm (eV) | integrated cross section[a] in eVÅ$^2$ | position (width) of Q band[b] in nm |
|---|---|---|---|---|---|
| CuPc | | 660 ± 2 (1.88 ± 0.01) | 27 (0.10) | 0.42 | 657.5 (57) |
| NiPc | | 657 ± 2 (1.89 ± 0.01) | 24 (0.09) | 0.35 | 651 (31) |
| $H_2Pc$ | $Q_y$ | 651 ± 2 (1.90 ± 0.01) | 30 (0.07) | 0.24 | 622.5 (73.5) |
| | $Q_x$ | 684 ± 2 (1.82 ± 0.01) | 19 (0.05) | 0.17 | 686 (38.5) |

[a] For experimental errors see text. [b] Vapor phase absorption data from ref 30.

with the band positions found in our study at 684 and 651 nm, respectively.

The integrated photodissociation cross section for the $Q_x$ and $Q_y$ band found for the free base phthalocyanine amount to 0.17 ± 0.02 eVÅ$^2$ and 0.24 ± 0.02 eVÅ$^2$, corresponding to an oscillator strength of 0.16 and 0.23, respectively. As discussed above, we conservatively estimate the absolute error to be a factor of 2. The total oscillator strength agrees reasonably with the values measured for $H_2Pc$ in solution (using 1-chloronaphthalene as solvent) of 0.22 and 0.18.[33] The experimental values fall somewhat short compared to recent ab initio CI calculations of the dipole allowed electronic excitations of $H_2Pc$ which suggest oscillator strengths of 1.05 and 0.585 for transitions at 1.3 and 1.51 eV, respectively.[34]

As a caveat one has to consider that photo*dissociation* cross sections can only be related to photo*absorption* cross sections, if competing relaxation channels can be neglected. Electronic luminescence is in principle such a possible channel leading to a systematic underestimate of the absorption cross section. It is well-known, e.g., from solution studies, that many phthalocyanines fluoresce upon excitation of the Q band. Interestingly, there is a strong dependence of the fluorescence quantum yield on the central metal atom. For the vapor phase, it was found that $H_2Pc$ as well the phthalocyanines with light metal atoms (Mg or Zn) exhibit fluorescence of at least 2 orders of magnitude higher quantum yield than CuPc.[35] Since the integrated cross sections obtained in this work are very similar for the tetraanionic analogues $H_2Pc(SO_3)_4^{4-}$ and $CuPc(SO_3)_4^{4-}$, we consider fluorescence to be an insignificant relaxation channel under the experimental conditions described.

The band further to the blue centered around 610 nm, which is observed for all three molecules (labeled Q′ in Figures 7-9) is most likely due to n → $\pi^*$ transitions as proposed recently[36] and stems from excitations of lone pair electrons at the nitrogen atoms. While a complete assignment of the spectra is beyond the scope of this manuscript, the spectral data provide clear evidence that our photodepletion method is in fact mapping the electronic band structure of the molecules studied by means of metastable decomposition after photon absorption.

So what is the role of the excess charges in these multiply charged anions? It is tempting to postulate that the excess charges localized at the sulfonate groups of the phthalocyanines do not strongly influence the optical response of the chromophore but rather act as an electrostatic corral as suggested recently[23,37] to give rise to metastable anionic states. These extra "spectator" charges are localized in molecular orbitals that seem to be sufficiently low lying in energy that they virtually do not interact with the valence electrons responsible for the lowest electronic excitations giving rise to the UV−vis spectra of these molecules − other than uniformly raising their energy relative to the vacuum level. On the other hand electronic excitation from an MO of the phthalocyanine scaffold can lead to a new decay channel: electron (tunneling) emission through the Coulomb barrier. The effective activation barriers are thereby lowered from 6.4 eV (the ionization potential of the neutral molecule[38]) to the effective barrier observed found in this work of about 2 eV.

Note that such excitation leaves behind a sort of zwitter ion that might be written as $MPc^+(SO_3^-)_4$. For the future, it will be of great interest to do (time-resolved) spectroscopic studies on the resulting trianion to test this hypothesis, particularly as there is solution phase data as well as computational information[39] on the expected shift in electronic excitation when charge is added into or withdrawn from the phthalocyanine moiety.

## 4. Conclusion

We report a photodissociation study of metastable tetraanionic phthalocyanine molecules isolated in a Penning trap. The experimental setup is described in detail and measurements are performed which indicate that electronic spectroscopy can be routinely performed at a reasonable duty cycle. Photodissociation probed at 355 nm as well as in the range 570−695 nm show that the investigated molecules fragment preferentially by electron emission, loss of the charge carrying $SO_3^-$ group, as well as $SO_2$ loss, leaving behind the intact phthalocyanine chromophore.

The results suggest that on average a two photon absorption process is sufficient to induce electron loss and fragmentation on the experimental time scale of 10 ms, thus allowing to get electronic spectra by monitoring the ion depletion as a function of wavelength for these large molecules. This is in contrast to electronic photodissociation probes of neutral or singly charged congeners for which higher excitation levels (requiring significantly more than two photons) are likely necessary.

We have shown herein that photodissociation of metastable multianions can be a useful approach for gas-phase electronic spectroscopy of large (embedded) chromophores provided that excess negative charges can be "attached", e.g., by chemical substitution, in such a way that they do not alter the electronic structure of the chromophore of interest. Due to the contribution of a tunneling channel, electron detachment from such systems is likely associated with lower effective activation energy than the classical barrier height. For the closed shell chromophores studied here, "perimeter charging" by $SO_3^-$ makes available a new *m*/*z* changing decay channel having activation energy of ca. 2 eV. As the chromophore itself has much higher energy decay channels, it becomes easier to perform absorption/depletion spectroscopy via the expedient of "charging up" the molecule. This may be generally applicable. Future work should also address the possibility of vibrational excitation of (cooled) metastable multianions to provide infrared spectra in either multiphoton one-color or two-color schemes via probes of electron detachment.

**Acknowledgment.** The authors thank Dr. Silviu Balaban for carefully reading the manuscript and useful comments. Support by the Strategiefond of the Helmholtz Foundation is gratefully acknowledged as is partial support by the DFG. M.M.K. thanks the Fonds der Chemischen Industrie for assistance.

## Appendix

We briefly derive the model equation used as eq 10 in the text which includes explicitely the laser beam and ion cloud profile starting with the two-photon absorption law

$$\frac{I}{I_0} = (1 + \sigma(\omega)F)\exp\{-\sigma(\omega)F\} \qquad \text{(A1)}$$

where $\sigma(\omega)$ is the energy dependent dissociation cross section and $F$ is the photon density. In the following the energy dependence of $\sigma$ will not be explicitly mentioned. Note that we have taken the overlap parameter $\alpha$ to be unity. We describe the local photon density with a normalized Gaussian ellipsoid

$$\Phi(x,y) = \frac{1}{\pi\, d_{Lx}\, d_{Ly}} \exp\left\{-\frac{x^2}{{d_{Lx}}^2} - \frac{y^2}{{d_{Ly}}^2}\right\} \qquad \text{(A2)}$$

where $d_{Lx}$ and $d_{Ly}$ are the widths of the photon density in $x$ and $y$ direction at the $e^{-1}$ level. $\Phi$ is here normalized to one, not to the total number of photons per pulse as one might expect, for further convenience. The ion cloud density is approximated by two overlapping Gaussians, as described in section 3.2, with eventual rotation by $2\pi$ around the symmetry axis to give a 3D cylindrically symmetric profile. Thus, we obtained

$$\rho(x,y) = \frac{N_0}{A} \exp\{-(\sqrt{x^2 + y^2} - r_0)^2/2{d_C}^2\} \qquad \text{(A3)}$$

where $N_0$ is the total number of ions present in the cloud, $r_0$ is the radius of the innermost circle from the origin to the maximum of the Gaussian profile, $d_C$ is the width of the profile at the $e^{-0.5}$ level, and $1/A$ is the factor which normalizes the profile obtained from analytical integration using polar coordinates

$$A = 2\pi{d_C}^2 \exp\left\{-\frac{{r_0}^2}{2{d_C}^2}\right\} + r_0 d_C \pi^{3/2}\sqrt{2}\left(1 + \mathrm{erf}\left\{\frac{r_0}{d_C\sqrt{2}}\right\}\right) \qquad \text{(A4)}$$

With the assumption that the integral absorption laws given above are still locally valid, the homogeneous photon density $F$ in equation A1 can be substituted by equation A2. The intensity ratio $I/I_0$ can be interpreted as the fraction of surviving precursor ions after the irradiation. It is then possible to substitute $I_0$ by equation A3 and $I$ by the number density of surviving precursor ions, and after integrating both sides over the whole surface and dividing by $N_0$, we obtain $I/I_0$ as

$$\frac{I}{I_0} = \int_{-\infty}^{\infty}\int_{-\infty}^{\infty} \rho(x,y)\left(1 + \sigma\frac{P}{h\nu}\Phi(x,y)\right) \times \exp\left\{-\sigma\frac{P}{h\nu}\Phi(x,y)\right\} \mathrm{d}x\, \mathrm{d}y \qquad \text{(A5)}$$

where $P$ is the integral laser pulse energy, $\nu$ is the frequency of the laser light, and $h$ is the Planck constant, thus $P/h\nu$ is the total number of photons per pulse. Since eq A5 cannot be solved analytically, it was solved numerically for each pair of $P$ and $I/I_0$ using the program package Mathematica.[40] We did so varying the parameters $d_{Lx}$ and $d_{Ly}$ every 10 nm which were reasonable steps to model the change in the laser beam's profile.

## References and Notes


(1) For a recent overview, see, for example: Dunbar, R. C. *Int. J. Mass Spectrom.* **2000**, *200*, 571.
(2) Dunbar, R. C. *J. Am. Chem. Soc.* **1970**, *93*, 5354.
(3) Freiser, B. S.; Beauchamp, J. L. *Chem. Phys. Lett.* **1975**, *35*, 35.
(4) Fu, E. W.; Dunbar, R. C. *J. Am. Chem. Soc.* **1978**, *100*, 2283.
(5) Hettich, R. L.; Jackson, T. C.; Stanko, E. M.; Freiser, B S. *J. Am. Chem. Soc.* **1987**, *108*, 5086.
(6) Dibben, M. J.; Kage, D.; Szczepanski, J.; Eyler, J. R.; Vala, M. *J. Phys. Chem. A* **2001**, *105*, 6024.
(7) Dunbar, R. C. *J. Chem. Phys.* **1991**, *95*, 2537.
(8) Dunbar, R. C.; McMahon, T. B. *Science* **1998**, *297*, 194.
(9) Andersen, J. U.; Hvelplund, P.; Nielsen, S. B.; Pedersen, U. V.; Tomita, S. *Phys. Rev. A* **2002**, *65*, 053202.
(10) Wang, X.-B.; Wang, L.-S. *Phys. Rev. Lett.* **1999**, *83*, 3402.
(11) Wang, X.-B.; Wang, L.-S. *Nature* **1999**, *400*, 245.
(12) Weber, J. M.; Ioffe, I. N.; Berndt, K. M.; Löffler, D.; Friedrich, J.; Ehrler, O. T.; Danell, A. S.; Parks, J. H.; Kappes, M. M. Submitted.
(13) Weis, P.; Hampe, O.; Gilb, S.; Kappes, M. M. *Chem. Phys. Lett.* **2000**, *321*, 426.
(14) Arnold, K.; Balaban, T. S.; Blom, M. N.; Ehrler, O. T.; Gilb, S.; Hampe, O.; van Lier, J. E.; Weber, J. M.; Kappes, M. M. *J. Phys. Chem. A* **2003**, *107*, 794.
(15) Blom, M. N.; Hampe, O.; Gilb, S.; Weis, P.; Kappes, M. M. *J. Chem. Phys.* **2001**, *115*, 3690.
(16) Gerlich, D. In *Advances in Chemical Physics*; Ng, Ch.-Y., Baer, M., Eds.; John Wiley and Sons Inc.: New York, 1992; Vol. LXXXII.
(17) M. Kordel, Diploma thesis, University of Karlsruhe, 2002.
(18) M. Neumaier, Diploma thesis, University of Karlsruhe, 2002.
(19) SIMION 6.0, Idaho National Lab.
(20) Friedrich, J., Gilb, S., Ehrler, O. T., Behrendt, A., Kappes, M. M. *J. Chem. Phys.* **2002**, *117*, 2635.
(21) Similar results were obtained for the $NiPc(SO_3)_4^{4-}$ ion with $\alpha = 0.99+-0.01$, $\gamma = 0.20+-0.05$ and $\sigma = 0.89+-0.05$ Å$^2$. Slight differences in cross-section are most likely due to variation in the position of the B band for the Ni homologue.
(22) Bréchignac, C.; Cahuzac, Ph.; Kebaili, N.; Leygnier, J.; Sarfati, A. *Phys. Rev. Lett.* **1992**, *68*, 3916.
(23) Wang, X.-B.; Ferris, K.; Wang, L.-S. *J. Phys. Chem. A* **2000**, *104*, 25.
(24) Klots, C. *Chem. Phys. Lett.* **1991**, *186*, 73.
(25) Compton, R. N.; Tuinman, A. A.; Klots, C. E.; Pederson, M. R.; Patton, D. C. *Phys. Rev. Lett.* **1997**, *78*, 4367.
(26) HyperChem Release 6.0, Hypercube Inc. 1999.
(27) Haarhoff, P. C. *Mol. Phys.* **1963**, *7*, 101.
(28) Hartig, J.; Blom, M. N.; Hampe, O.; Kappes, M. M. *Int. J. Mass Spec.* **2003**, *229*, 93.
(29) Depending on the wavelength, one thereby obtaines ratios $\sigma_2/\sigma_1$ of up to 10, where it cannot be distinguished between the first and the second photon.
(30) Edwards, L.; Gouterman, M. *J. Mol. Spectrosc.* **1970**, *33*, 292.
(31) Bondybey, V. E.; English, J. H.; *J. Am. Chem. Soc.* **1979**, *101*, 3446.
(32) Huang, T.-H.; Rieckhoff, K. E.; Voigt, E. M. *J. Chem. Phys.* **1982**, *77*, 3424.
(33) Day, P. N.; Wang, Z.; Pachter, R. *J. Mol. Struct. (THEOCHEM)* **1998**, *455*, 33 and references therein.
(34) Toyota, K.; Hasegawa, J.; Nakatsuji, H.; *J. Phys. Chem. A* **1997**, *101*, 446.
(35) Eastwood, D.; Edwards, L.; Gouterman, M.; Steinfeld, J. *J. Mol. Spectrosc.* **1966**, *20*, 381.
(36) Mack, J.; Stillman, M. J. *Inorg. Chem.* **2001**, *40*, 812 and references therein.
(37) Simons, J.; Skurski, P.; Barrios, R. *J. Am. Chem. Soc.* **2000**, *122*, 11893.
(38) Berkowitz, J. *J. Chem. Phys.* **1979**, *70*, 2819.
(39) Liao, M.-S.; Scheiner, S. *J. Chem. Phys.* **2001**, *114*, 9780.
(40) Mathematica, version 4.1, Wolfram Research, 1999.